ACSNANO
www.acsnano.org
ARTICLE

Enhancing the Efficiency of Silicon-Based Solar Cells by the Piezo-Phototronic Effect

Laipan Zhu,[†,⊥] Longfei Wang,[†,⊥] Caofeng Pan,[†] Libo Chen,[†] Fei Xue,[†] Baodong Chen,[†] Leijing Yang,[†] Li Su,[†] and Zhong Lin Wang*[,†,‡]

[†]Beijing Institute of Nanoenergy and Nanosystems, Chinese Academy of Sciences, National Center for Nanoscience and Technology (NCNST), Beijing 100083, China

[‡]School of Material Science and Engineering, Georgia Institute of Technology, Atlanta, Georgia 30332, United States

Supporting Information

ABSTRACT: **Although there are numerous approaches for fabricating solar cells, the silicon-based photovoltaics are still the most widely used in industry and around the world. A small increase in the efficiency of silicon-based solar cells has a huge economic impact and practical importance. We fabricate a silicon-based nanoheterostructure (p^+-Si/p-Si/n^+-Si (and n-Si)/n-ZnO nanowire (NW) array) photovoltaic device and demonstrate the enhanced device performance through significantly enhanced light absorption by NW array and effective charge carrier separation by the piezo-phototronic effect. The strain-induced piezoelectric polarization charges created at n-doped Si-ZnO interfaces can effectively modulate the corresponding band structure and electron gas trapped in the n^+-Si/n-ZnO NW nanoheterostructure and thus enhance the transport process of local charge carriers. The efficiency of the solar cell was improved from 8.97% to 9.51% by simply applying a static compress strain. This study indicates that the piezo-phototronic effect can enhance the performance of a large-scale silicon-based solar cell, with great potential for industrial applications.**

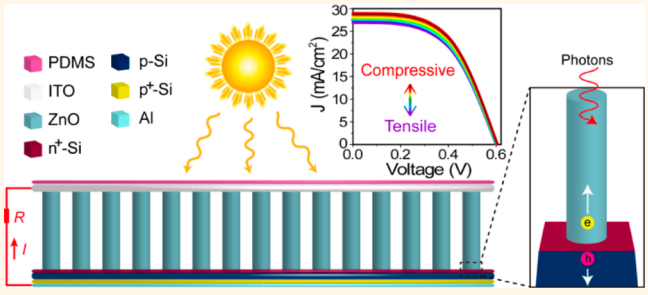

KEYWORDS: *silicon-based solar cell, ZnO nanowire array, light absorption, piezo-phototronic effect, piezopotential*

For decades, the silicon-based solar cell has been intensively investigated, owing to the commercial applications.[1−5] The use of ion implantation for selective area doping is one of the critical technologies for advancement of silicon-based solar cells.[3,6−8] The technique offers several advantages over conventional phosphoric trichloride ($POCl_3$) and in-line diffusion technologies including fewer process steps, high-throughput manufacturing process, *in situ* oxidation for superior surface passivation, precise doping control, and advanced dopant profile engineering by varying implantation dose, implantation energy, and implant damage annealing recipe, *etc.*[3,9,10] However, light absorption, electron−hole pair separation, surface/interface recombination, and surface barrier (induced by the Gaussian distribution of implanted ions) are four main factors limiting the efficiency of silicon-based solar cells.[1−3,11]

Antireflective coatings and light trapping are two established ways to enhance light absorption and hence increase the amount of photoexcited carriers in the absorption layer.[11−16] Recently, nanowire (NW) arrays have revealed potential benefits with broadband antireflective and light trapping properties in thin-film solar cells,[17−20] which eliminates the requirement for conventional complex expensive vacuum-deposited antireflection coatings. Meanwhile, using piezoelectric semiconductor NWs that typically have wurtzite structure (such as ZnO, CdS, and GaN), the piezo-phototronic effect has been proven to be an effective approach to improve the separation of photoinduced electron−hole pairs, suppress the nonradiative recombination, and significantly enhance the performance of photovoltaic (PV) devices.[21−30] In these former studies, piezo-phototronic effect is generally used to enhance the performance of PV devices based on single NW. Upon normal stress, owing to the noncentral symmetric crystal structure, the piezoelectric polarization charges induced piezopotential in the NW at the heterojunction or interface can act as a "gate" voltage to modulate the band structure of heterojunction and tune the charge separation, transport, and/or recombination in optoelectronic processes, leading to either an enhancement or reduction of the photocurrent.[21,22,31−34]

In this article, we developed several ion-implanted monocrystalline silicon solar cells with enhanced efficiency,

Received: November 27, 2016
Accepted: January 13, 2017
Published: January 13, 2017

DOI: 10.1021/acsnano.6b07960
ACS Nano 2017, 11, 1894−1900

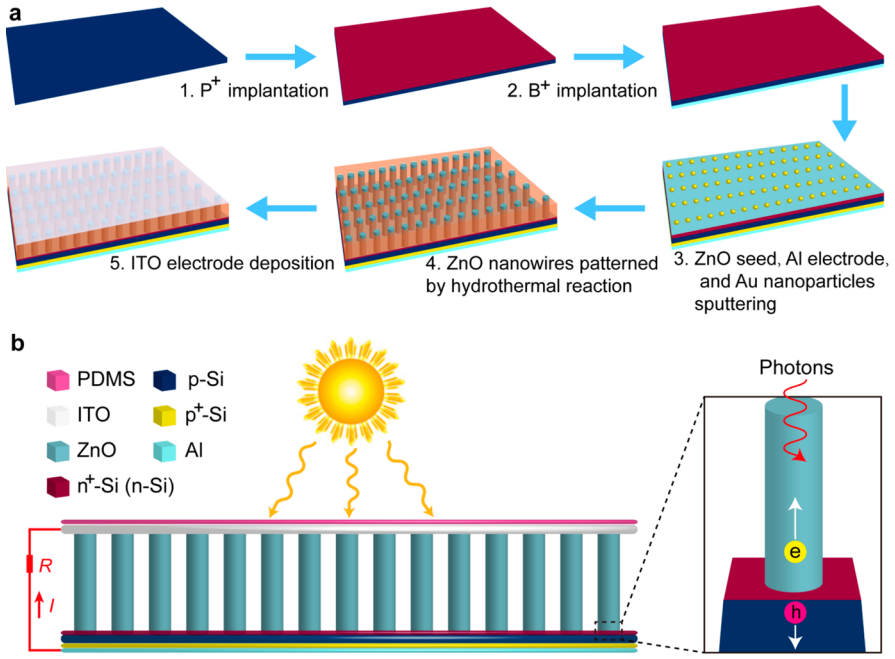

Figure 1. Silicon-based nanoheterstructure solar cell layout. (a) Schematic diagrams illustrating the fabrication process of the patterned silicon-based nanoheterostructure solar cell. (b) Schematic of the solar cell. Under illumination, photoexcited electron−hole pairs are produced and subsequently separated at the n-ZnO nanowire/n^+-Si (n-Si)/p-Si interface because of band bending and internal field. The electrons then move to the ZnO nanowire, and holes move to the p-Si.

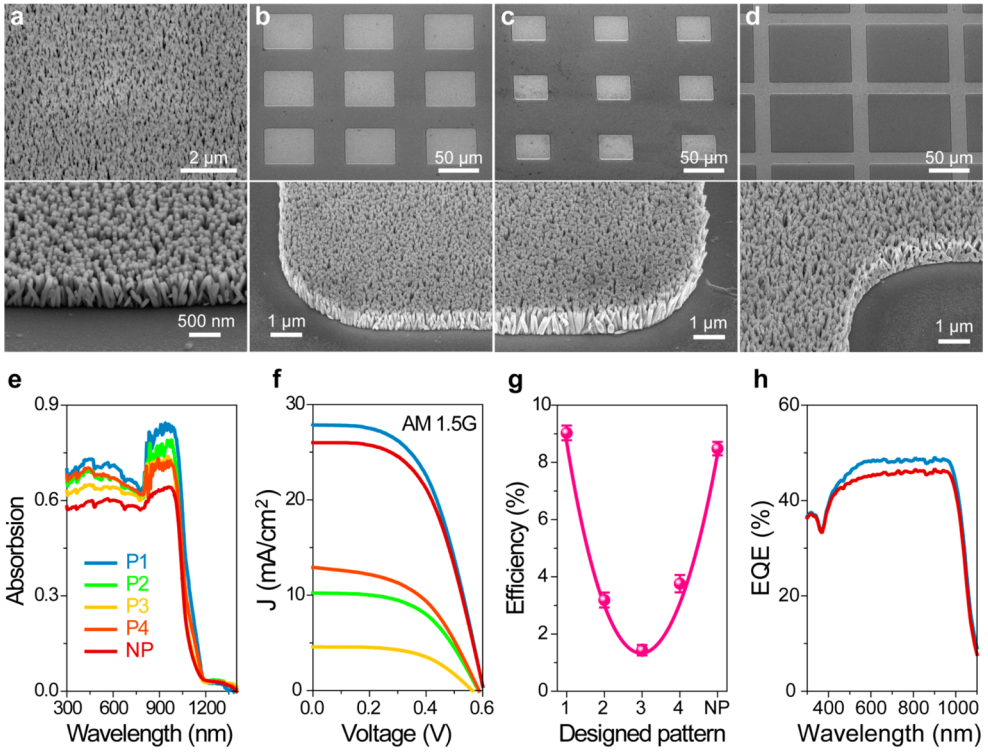

Figure 2. Comparison of the performance of four kinds of solar cells with different n-ZnO nanowire array patterns. (a−d) SEM images of the four samples with different n-ZnO nanowire array patterns grown on the top of Si p−n^+ junction through photolithography and low-temperature hydrothermal reaction. The designed patterns are defined as P1, P2, P3, and P4, respectively, from the left to the right. The SEM images in the upper row are low magnification, and the SEM images in the lower row are high magnification. (e) Absorption spectra of the solar cells with different n-ZnO NW array patterns, where NP denotes the compared solar cells with no pattern. (f) *J*−*V* characteristics of the solar cells under AM 1.5G illumination. (g) The solar energy conversion efficiency of the solar cells with different designed patterns. (h) EQE spectra of solar cells with pattern P1 (blue line) and pattern NP (dark brown line).

owing to the decoration of ZnO NW arrays (Figure 1b). The ZnO NW arrays can effectively enhance the light absorption, and the strain-induced piezoelectric polarization charges created at n-doped Si-ZnO interfaces effectively modulate the

DOI: 10.1021/acsnano.6b07960
ACS Nano 2017, 11, 1894−1900

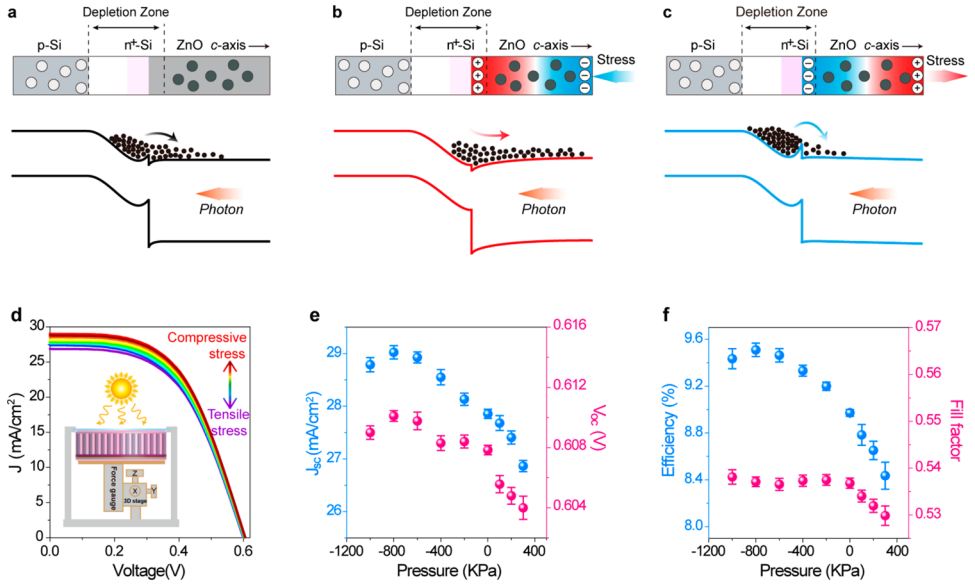

Figure 3. Performance and proposed mechanism of the p$^+$-Si/p-Si/n$^+$-Si/n-ZnO nanowire array solar cell with pattern P1 under various vertical pressures. (a) Energy band diagram of the solar cell without stress. (b) Energy band diagram of the solar cell after applying a compressive stress on the PV device, which shows modulation effect on the band structure of n$^+$-Si/ZnO interface and electron gas trapped in n$^+$-Si/ZnO NW heterojunction by strain-induced positive polarization charges. (c) Energy band diagram of the solar cell after applying a tensile stress on the PV device, which shows a modulation effect on the band structure of n$^+$-Si/ZnO interface and electron gas trapped in n$^+$-Si/ZnO NW heterojunction by strain-induced negative polarization charges. (d–f) Vertical pressure dependence of the *J*–*V* characteristics, the short-circuit current density, the open-circuit voltage, the fill factor, and the efficiency under AM 1.5G illumination, which indicates the modulation of carrier transport by piezo-phototronic effect. The negative pressure means compressive strain, and positive pressure means tensile strain. Inset: Schematic cross-section diagram of the solar cell under a vertical stress.

corresponding band structure and electron gas trapped in n$^+$-Si, and thus enhance the separation of photoinduced carriers. Our devices show an enhanced efficiency from 8.97% to 9.51% by simply applying a static compress strain.

RESULTS AND DISCUSSION

The fabrication process of silicon-based nanoheterostructure solar cells is shown in Figure 1a. The photovoltaic devices were packaged into polydimethylsiloxane (PDMS) to enhance the mechanical property and avoid cracking of NW arrays so that the vertical pressure can be softly applied on the NW arrays (Supporting Information Figure S1). First, four kinds of PV devices with different ZnO NW array patterns grown on the top of a Si p–n$^+$ junction through photolithography and low-temperature hydrothermal reaction were fabricated for comparison (see Figure 2a–d and Supporting Information Figure S2). The as-grown ZnO nanowires were ∼1 μm long and ∼100 nm in diameter. From the absorption spectra shown in Figure 2e, the devices with pattern P1 (ZnO NW array completely covering the top surface of p-Si/n$^+$-Si junction) possess the highest absorption efficiency, and the devices with no pattern (NP) have the smallest absorption efficiency, which illustrates that ZnO NW arrays can effectively serve as antireflective coating and light trapping structures and hence effectively enhance light absorption. The *J*–*V* characteristics of the optimal PV devices were measured under AM 1.5G illumination (Figure 2f), which denotes that the devices with the pattern P1 shows the best performance. The efficiency (η) of silicon-based nanoheterostructure solar cells with pattern P1 is about 9%, which is a bit larger than even the solar cells with no pattern, while the efficiencies of those with P2, P3, and P4 are no more than 4% (see Figure 2g). First, it is due to that it is more sufficient to the electrical collection of photoexcited carriers for NW arrays with larger area patterns, which means that the devices with a larger size of top electrodes are beneficial to the device performance. Second, although NW arrays reduce the collecting ability of photoexcited carriers compared to the solar cells with no pattern, the effect of enhanced light absorption exceeds the effect of reduced carrier collection for pattern P1, while it does not for patterns P2, P3, and P4. The external quantum efficiency (EQE) of the devices with pattern P1 was measured to be a bit larger than those with no pattern (Figure 2h), illustrating an enhanced performance profits from the modification of ZnO NW arrays. The performance of the devices with pattern P1 under different illumination intensity (*P*) is also shown in the Supporting Information (Figure S3 and Supporting Information Note 1), in which the calculated η is enhanced from 6.8% to 9% with the illumination intensity increasing from 20 to 100 mW/cm^2, indicating that the photoexcited electron–hole pairs can also be sufficiently separated at the silicon homojunction interface even under higher illumination intensity.[27,35] It is worth noting that the performance of such p-Si/n$^+$-Si/n-ZnO nanowire array solar cells can be enhanced by optimizing the density, size, and length of the ZnO nanowires, the thickness and doping level of the silicon substrate, and the metal–semiconductor contact, *etc.*

To investigate the effects of the piezopotential on the performance of the p$^+$-Si/p-Si/n$^+$-Si/n-ZnO nanowire array solar cells with pattern P1, the PV devices encapsulated with PDMS were fixed on a high-transparent acrylic by superglue in order to bear the vertical pressures. To be noted, when pulling the sample, a tensile pressure would be completely applied to the PDMS but partially transmitted to the ZnO NWs. Although the tensile pressure on the ZnO NWs is much smaller than that on the PDMS, it still affects the performance of the devices. The pressures shown in all figures denote the pressures on

DOI: 10.1021/acsnano.6b07960
ACS Nano 2017, 11, 1894–1900

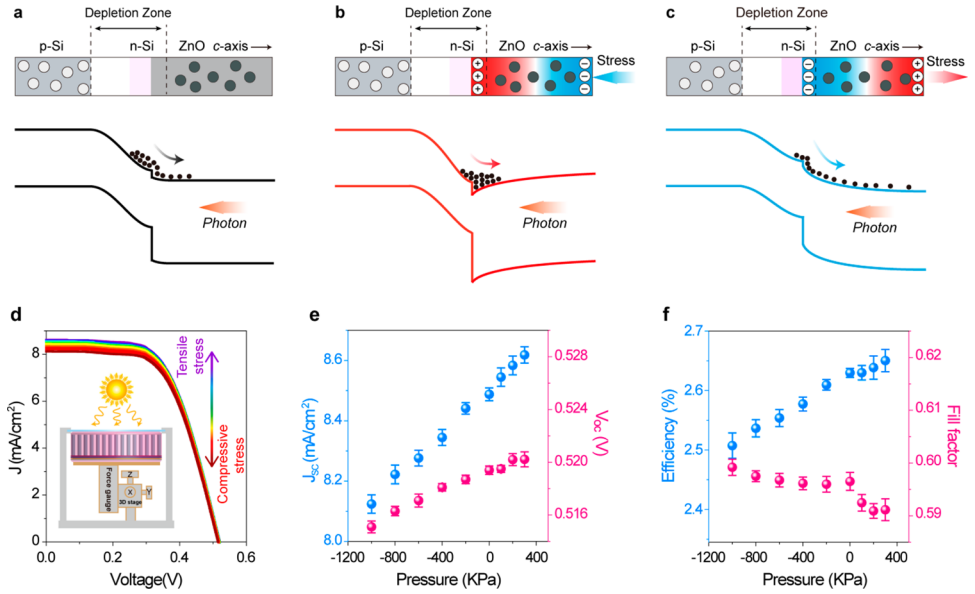

Figure 4. Performance and proposed mechanism of the p$^+$-Si/p-Si/n-Si/n-ZnO nanowire array solar cell under various vertical pressures. (a) Energy band diagram of the solar cell without stress. (b) Energy band diagram of the solar cell after applying a compressive stress on the PV device, which shows modulation effect on band structure of n$^+$-Si/ZnO interface by strain-induced positive polarization charges. (c) Energy band diagram of the solar cell after applying a tensile stress on the PV device, which shows a modulation effect on band structure of n$^+$-Si/ZnO hererojunction by strain-induced negative polarization charges. (d–f) Vertical pressure dependence of the *J*–*V* characteristics, the short-circuit current density, the open-circuit voltage, the fill factor, and the efficiency under AM 1.5G illumination, which indicate the modulation of carrier transport by piezo-phototronic effects. Inset: Schematic cross-section diagram of the solar cell under a vertical stress.

PDMS but not on ZnO NWs. The *J*–*V* characteristics of the solar cells under a variety of vertical pressures (−1000 to 300 KPa on the PDMS, where negative and positive signs, respectively, denote compressive and tensile pressures) were measured under AM 1.5G illumination, as shown in Figure 3d. Specifically, the J_{SC}, V_{OC}, and fill factor (FF) under different vertical pressures are extracted and plotted (Figure 3e,f). When the compressive pressure adds up to ∼800 KPa, the J_{SC} increases from 27.86 to 29.03 mA/cm^2, the V_{OC} increases from 0.6078 to 0.6101 V, and the FF increases slightly from 0.5368 to 0.5381. As a result, the solar energy conversion efficiency is enhanced from 8.97% to 9.51% when a compressive pressure of ∼800 KPa is applied. When the compressive pressure further increases, however, the efficiency begins to fall off. When the tensile pressure adds up to 300 KPa, it can be found that the J_{SC} decreases from 27.86 to 26.86 mA/cm^2, and the V_{OC} decreases from 0.6078 to 0.604 V, and the FF decreases from 0.5368 to 0.5299. As a result, the efficiency is reduced from 8.97% to 8.44% when a 300 KPa tensile pressure is applied. The mechanisms of piezopotential tuning the performance of silicon-based solar cells are detailed as following.

The ion implantation technique and the distribution of phosphorus ion (P$^+$) with implanted energy of 80 keV and dose of 10^{15} cm^{-2} in the heavy-doped n$^+$-Si solar cell are detailed in the Supporting Information (Figure S4 and Supporting Information Note 2), from which we can see that the concentration of ions in the implanted depth follows a Gaussian distribution, the maximum concentration is 1 × 10^{20} cm^{-3}, and the maximum implanted depth is about 230 nm. The width of the built-in electric field in n-type Si can be expressed as[35]

$$x_n = \frac{N_A}{N_A + N_D}\sqrt{V_D\left(\frac{2\varepsilon_r\varepsilon_0}{q}\right)\left(\frac{N_A + N_D}{N_A N_D}\right)}$$

where N_A, N_D, V_D, ε_r, ε_0, and q are the acceptor concentration, the donor concentration, the contact potential difference, the relative dielectric constant, the vacuum dielectric constant, and the elementary charge, respectively. In general, V_D = 0.75 V and ε_r = 11.9 are selected for Si. For the heavy-doped solar cell with $N_A = 10^{16}$ cm^{-3} and $N_D = 10^{18}$–10^{20} cm^{-3}, x_n is calculated to be about several nanometers, which denotes the depletion zone is quite narrow in n$^+$-Si, and it mainly locates in p-Si. Hence, the strong inner electric field in Si p–n$^+$ junction could not affect the energy band of n$^+$-Si/n-ZnO junction. As the density of the ion implanted P$^+$ is lower at the surface than at the inner part of n$^+$-Si, the energy band level at the surface of n$^+$-Si will be raised up, and as a result there will be a surface barrier, and hence a large portion of photoexcited electrons are trapped in the middle of n$^+$-Si; the energy band diagram is illustrated as shown in Figure 3a. When a compressive pressure is applied on the device, due to the polar *c*-axis orientation in NWs, piezopotential distributes along the ZnO NWs with positive piezoelectric polarization charges appearing at the junction, which can further lower the energy level of the depletion zone between n$^+$-Si and n-ZnO, hence the trapped electrons in n$^+$-Si will be released to n-ZnO (Figure 3b), which is equivalent to an increased generation rate of photon-induced carriers. The flow of trapped electrons results in a temporary increase of J_{SC} and V_{OC}. What's more, with the decrease of the parasitic resistance of the device, FF will increase. Therefore, the efficiency is calculated to increase (Figure 3f). Actually, the change in J_{SC}, V_{OC}, and FF is not obvious under such strains, which is due to the piezo-electric charges at the end of ZnO NWs that are partially screened by the light-induced free charges.[26,36−39] However, when the compressive pressure exceeds ∼800 KPa or

DOI: 10.1021/acsnano.6b07960
ACS Nano 2017, 11, 1894–1900

the trapped electrons are all released, the tilted band starts to slow down the transport of electrons due to the enhanced piezopotential as well as the deepened triangular quantum well in ZnO NW, thus the efficiency begins to fall off with the further increase in compressive pressure (Figure 3f).

When a tensile stress is applied on the device, negative piezoelectric polarization charges present at the bottom surfaces, distributing within a thickness of 1−2 atomic layers, which will further lift up the energy level of the depletion zone between n^+-Si and n-ZnO (Figure 3c), which greatly increased the trapping of the photon generated electrons. Similarly analyzing as the above, the J_{SC}, V_{OC}, and FF are all decreased, hence the efficiency is reduced with the increase of tensile pressure (Figure 3f).

As a comparison, we studied the performance of a solar cell with low-doped n-Si (P^+ implantation with energy of 40 keV and dose of 1.5×10^{11} cm^{-2}), that is, the fabrication process of the two devices (low-doped n-Si solar cell and heavy-doped n^+-Si solar cell) is the same except for the doping level of n-type Si. The efficiency of the PV device with p^+-Si/p-Si/n-Si/n-ZnO NW array nanoheterostructure was measured at only about 2.63% without stress, which is much lower than that of the above heavy-doped n^+-Si solar cell. The vertical pressure dependence of the $J-V$ characteristics of the solar cell was measured under AM 1.5G illumination, as shown in Figure 4d. With the measured pressure changing from −1000 to 300 KPa, the J_{SC} increased almost linearly from 8.12 to 8.62 mA/cm^2, the V_{OC} increases almost linearly from 0.5151 to 0.5202 V, the FF decreases slightly from 0.6 to 0.59. As a result, the calculated efficiency is increased weakly under tensile pressures while restrained under compressive pressures. The changing tendency is totally different from the above heavy-doped n^+-Si solar cells. These changing tendencies are in agreement with the result expected from the piezo-phototronic model, to be presented.

For this light-doped n-Si solar cell with an implanted energy of 40 keV and a dose of 1.5×10^{11} cm^{-2}, the distribution of the density of the implanted phosphorus ions is shown in Figure S4, Supporting Information, where we can see that the concentration of ions in the implanted depth follows a Gaussian distribution, the maximum concentration is 2×10^{16} cm^{-3}, and the maximum implanted depth is about 125 nm. For this light-doped solar cell with $N_A = 10^{16}$ cm^{-3} and $N_D = 1 \times 10^{14}$ to 2×10^{16} cm^{-3}, the width of the built-in electric field in n-Si is estimated to be $x_n \sim 130$ nm, which exceeded the estimated maximum implanted depth of 125 nm. Namely, the positive space charges in n-Si are not enough to neutralize the negative space charges in p-Si. Therefore, the strong inner electric field in the p-Si/n-Si junction will extend to n-Si/n-ZnO junction (Figure 4a−c). On this occasion, there will be no surface barrier in n-Si and hence no photon-excited electrons being trapped in the middle of n-Si, which is different from the former heavy-dopped case in Figure 3. Note the absolute photon generated current here is about 1/3 of that in Figure 3e for the heavy doping case. When the device was subjected to an external compressive mechanical deformation, the positive piezoelectric charge will lower the energy level of the depletion zone between n-Si and n-ZnO NW and lift up the energy level near the other side of n-ZnO NW with negative piezoelectric charges (Figure 4b). As a result, the separation and transport of photoexcited carriers are suppressed, owing to the local trapping at the junction and the tilted band by piezo-phototronic effect, hence J_{SC} and V_{OC} are all decreased. Although FF is still increased slightly with the decrease of the parasitic resistance, the calculated efficiency drops with the increase of compressive pressure, as observed experimentally in Figure 4d,e.

On the contrary, when a tensile pressure is applied on the device (Figure 4c), the negative piezoelectric charges will lift up the energy level of the depletion zone between n-Si and n-ZnO and lower the energy level at the other end of n-ZnO with the positive piezoelectric charges. The J_{SC} and V_{OC} are increased for the eliminated trapping at the junction and increased the charge separation, while FF decreases largely with the increase of the parasitic resistance. Therefore, the calculated efficiency increases with the increase in tensile pressure, as verified experimentally in Figure 4f.

CONCLUSIONS

In summary, some silicon-based nanoheterostructure (p^+-Si/p-Si/n^+-Si (and n-Si)/n-ZnO NW array) photovoltaic devices with enhanced efficiency have been designed. The ZnO nanowire arrays can significantly enhance light absorption through light antireflection and trapping, and the strain-induced piezoelectric polarization charges at the n^+-Si/ZnO NW interface can effectively modulate the band structure of n^+-Si (n-Si)/ZnO NW nanoheterostructure and the electron gas trapped in n^+-Si and n^+-Si/n-ZnO NW heterojunction, thus enhance the charge carrier transport. As a result, the performance of the p^+-Si/p-Si/n^+-Si/n-ZnO NW array solar cells is enhanced from 8.97% to 9.51% when subjected to a 800 KPa static compressive pressure. There is still ample opportunity to further increase the efficiency of the silicon-based nanoheterostructure solar cells by the piezo-phototronic effect through using a better controlled structure and morphology of piezoelectric semiconductor nanomaterial. This study indicates a good method of optimizing performance of large-scale commercial solar cells (such as polycrystalline silicon solar cells, CIGS solar cells, and perovskite solar cells) *via* the piezo-phototronic effect.

METHODS

Fabrication Processes of the Solar Cells. First, two (001) monocrystal p-type Si wafers with a resistance of 1 Ω·cm, concentration of 10^{16} cm^{-3}, and thickness of 500 μm were prepared. Phosphorus ion (P^+) implantation with an energy of 80 keV and a dose of 1×10^{15} cm^{-2} was then carried out for heavy-doped n^+-Si in one of the p-type Si wafer at room temperature. P^+ implantation with energy of 40 keV and dose of 1.5×10^{11} cm^{-2} was carried out for low-doped n-Si in the other p-type Si wafer at room temperature. Then the back of the two p-type Si wafers was implanted with boron ion (B^+) with an energy of 80 keV and a dose of 1×10^{15} cm^{-2} for heavy-doped p^+-Si. These implantations were all processed in an ion implanter with type of HVE 400 kV. Then, the ion implanted monocrystalline silicon wafers were cut into squares of 1 cm × 1 cm and annealed at 900 °C for 30 s to repair the lattice damage and activate impurities in a rapid thermal processing (RTP) system. In order to remove the native oxide layer (SiO_2), the annealed samples were dipped in hydrofluoric acid with a mass fraction of 5% for 5 min, then ultrasonically cleaned by alcohol, acetone, and deionized water in sequence, and then dried with a nitrogen gun. The ZnO seed layer was deposited on the n^+-Si (or n-Si) by radio frequency (RF) magnetron sputtering (Denton Discovery 635, 40 sccm Ar, 100 W, 15 min) at room temperature. Au nanoparticles were deposited on the ZnO seed layer by a Sputter Coater/Cressington/Auto108 (20 mA, 10 s) at room temperature. And the Al bottom electrode was then deposited on the p^+-Si by direct current (DC) magnetron sputtering (Denton Discovery 635, 40 sccm Ar, 100 W, 10 min) at room temperature. The samples were then annealed in nitrogen at 300 °C for 3 min for ohmic contact. For

DOI: 10.1021/acsnano.6b07960
ACS Nano 2017, 11, 1894−1900

samples with patterns of P2, P3, and P4 (not including P1), a lithography process was used for different patterns to provide for the upcoming nanowire growth. In concrete terms, a SUN-9i negative photoresist of 1.5 μm was first spin-coated on the ZnO seed layer and then processed in turn with prebaking (110 °C, 90 s), exposure (5 s), postbaking (135 °C, 60 s), and development (30 s). Then, all the samples were placed into a mixed nutrient solutions (30 mM/L $Zn(NO_3)_2$ and 30 mM/L hexamethylenetetramine (HMTA)) at 80 °C for 3 h for the growth of ZnO nanowire arrays. To improve the mechanical property of the nanowires with pattern P1, the as-synthesized ZnO nanowire arrays were then spin-coated by poly(methyl methacrylate) (PMMA), followed by Ar plasma etching to expose the heads of the nanowires. A kind of PV device with no pattern (NP) was fabricated with an Al bottom electrode. Then, the ITO top electrode (40 sccm Ar, 100 W, 50 min) was then deposited on the top of the devices for all the samples by RF magnetron sputtering at room temperature. Two Cu wires were, respectively, attached on the ITO top electrode and the Al bottom electrode by silver-epoxy adhesive. Then, the devices were completely encapsulated with PDMS with thickness of ~1 mm on the top electrode and ~200 μm on the bottom electrode. In order to bear the vertical pressures, the PV devices with a pattern P1 were fixed on a high-transparent acrylic with superglue. A tension gauge was finally fixed on the bottom of the device with superglue.

Characterization and Measurement. The detailed microscopic structural and morphological characterizations were carried out with a HITACHI SU8020 field-emission scanning electron microscope (FESEM). The absorption spectra were obtained with an UV−vis-NIR spectrophotometer (SHIMADZU UV3600). The solar cells were irradiated using a solar simulator (Model 94023A, Newport) with an AM 1.5G spectrum distribution calibrated against a NREL reference cell to accurately simulate full-sun intensity (100 mW/cm^2). The EQE spectra were measured by a quantum efficiency measurement system (QEPVSI-b, Newport). A digital push and pull tester (HP-300) was applied to provide vertical pressures. The $J-V$ characteristics of the devices were recorded by an electrochemical workstation (CHI660E).

ASSOCIATED CONTENT

Supporting Information

The Supporting Information is available free of charge on the ACS Publications website at DOI: 10.1021/acsnano.6b07960.

Additional experimental details and data (PDF)

AUTHOR INFORMATION

Corresponding Author

*E-mail: zhong.wang@mse.gatech.edu.

ORCID

Zhong Lin Wang: 0000-0002-5530-0380

Author Contributions

⊥These authors contributed equally to this work.

Notes

The authors declare no competing financial interest.

ACKNOWLEDGMENTS

This research was supported by the "thousands talents" program for a pioneer researcher and his innovation team, China, National Natural Science Foundation of China (grant nos. 51432005, 5151101243, and 51561145021), the National Key R & D Project from Minister of Science and Technology (2016YFA0202704), the National Program for Support of Top-Notch Young Professionals, and the China Postdoctoral Science Foundation (2016M600067).

REFERENCES

(1) Green, M. A. The Path to 25% Silicon Solar Cell Efficiency: History of Silicon Cell Evolution. *Prog. Photovoltaics* **2009**, *17*, 183−189.

(2) Polman, A.; Knight, M.; Garnett, E. C.; Ehrler, B.; Sinke, W. C. Photovoltaic Materials. *Science* **2016**, *352*, aad4424.

(3) Rohatgi, A.; Meier, D. Developing Novel Low-Cost, High-Throughput Processing Techniques for 20%-Efficient Monocrystalline Silicon Solar Cells. *Photovoltaics Int.* **2010**, *10*, 87−93.

(4) Bullock, J.; Hettick, M.; Geissbühler, J.; Ong, A. J.; Allen, T.; Sutterfella, C. M.; Chen, T.; Ota, H.; Schaler, E. W.; De Wolf, S.; et al. Efficient Silicon Solar Cells with Dopant-Free Asymmetric Heterocontacts. *Nature Energy* **2016**, *1*, 15031.

(5) Blakers, A. W.; Wang, A.; Milne, A. M.; Zhao, J.; Green, M. A. 22.8% Efficient Silicon Solar Cell. *Appl. Phys. Lett.* **1989**, *55*, 1363−1365.

(6) Springer Series in Electrophysics. *Ion Implantation: Equipment and Techniques*; Ryssel, H., Glawischnig, H., Eds.; Springer-Verlag: Berlin, 1983; Vol. *11*, pp13−17.

(7) Anders, A. *Handbook of Plasma Immersion Ion Implantation and Deposition*. John Wiley & Sons, Inc.: New York, 2000.

(8) Ziegler, J. F. *Ion Implantation: Science and Technology*; Academic Press, Inc.: San Diego, CA, 1996.

(9) Krygowski, T.; Rohatgi, A. A Simultaneously Diffused, Textured, *In Situ* Oxide AR-Coated Solar Cell Process (STAR Process) for High-Efficiency Silicon Solar Cells. *IEEE Trans. Electron Devices* **1998**, *45*, 194−199.

(10) Rudolph, D.; Peter, K.; Meijer, A.; Doll, O.; Köhler, I. Etch Back Selective Emitter Process with Single POCL 3 Diffusion. In Proceedings from the *26th European PVSEC*, Hamburg, Germany, September 5−9, 2011; WIP Wirtschaft und Infrastruktur GmbH & Co.: Munich, Germany, 2011; pp 1349−1352.

(11) Brongersma, M. L.; Cui, Y.; Fan, S. Light Management for Photovoltaics Using High-Index Nanostructures. *Nat. Mater.* **2014**, *13*, 451−460.

(12) Rahman, A.; Ashraf, A.; Xin, H.; Tong, X.; Sutter, P.; Eisaman, M. D.; Black, C. T. Sub-50-nm Self-Assembled Nanotextures for Enhanced Broadband Antireflection in Silicon Solar Cells. *Nat. Commun.* **2015**, *6*, 5963.

(13) Oh, J.; Yuan, H.-C.; Branz, H. M. An 18.2%-Efficient Black-Silicon Solar Cell Achieved through Control of Carrier Recombination in Nanostructures. *Nat. Nanotechnol.* **2012**, *7*, 743−748.

(14) Battaglia, C.; Hsu, C.-M.; Söderström, K.; Escarré, J.; Haug, F.-J.; Charrière, M.; Boccard, M.; Despeisse, M.; Alexander, D. T. L.; Cantoni, M.; Cui, Y.; Ballif, C. Light Trapping in Solar Cells: Can Periodic Beat Random? *ACS Nano* **2012**, *6*, 2790−2797.

(15) Campbell, P.; Green, M. A. Light Trapping Properties of Pyramidally Textured Surfaces. *J. Appl. Phys.* **1987**, *62*, 243−249.

(16) Wang, P. H.; Nowak, R.-E.; Geißendörfer, S.; Vehse, M.; Reininghaus, N.; Sergeev, O.; von Maydell, K.; Brolo, A. G.; Agert, C. Cost-Effective Nanostructured Thin-Film Solar Cell with Enhanced Absorption. *Appl. Phys. Lett.* **2014**, *105*, 183106.

(17) Aé, L.; Kieven, D.; Chen, J.; Klenk, R.; Rissom, T.; Tang, Y.; Lux-Steiner, M. C. ZnO Nanorod Arrays as An Antireflective Coating for Cu(In,Ga)Se_2 Thin Film Solar Cells. *Prog. Photovoltaics* **2010**, *18*, 209−213.

(18) Lee, Y.-J.; Ruby, D. S.; Peters, D. W.; McKenzie, B. B.; Hsu, J. W. P. ZnO Nanostructures as Efficient Antireflection Layers in Solar Cells. *Nano Lett.* **2008**, *8*, 1501−1505.

(19) Nowak, R.-E.; Vehse, M.; Sergeev, O.; von Maydell, K.; Agert, C. ZnO Nanorod Arrays as Light Trapping Structures in Amorphous Silicon Thin-Film Solar Cells. *Sol. Energy Mater. Sol. Cells* **2014**, *125*, 305−309.

(20) Nowak, R.-E.; Vehse, M.; Sergeev, O.; Voss, T.; Seyfried, M.; von Maydell, K.; Agert, C. ZnO Nanorods with Broadband Antireflective Properties for Improved Light Management in Silicon Thin-Film Solar Cells. *Adv. Opt. Mater.* **2014**, *2*, 94−99.

(21) Wang, Z. L. Piezopotential Gated Nanowire Devices: Piezotronics and Piezo-Phototronics. *Nano Today* **2010**, *5*, 540−552.

DOI: 10.1021/acsnano.6b07960
ACS Nano 2017, 11, 1894−1900

(22) Wang, Z. L. Progress in Piezotronics and Piezo-Phototronics. *Adv. Mater.* **2012**, *24*, 4632−4646.
(23) Wang, Z. L. Piezo-Phototronic Effect on Solar Cells. *Microtechnology & Mems* **2012**, 153−178.
(24) Hu, G.; Guo, W.; Yu, R.; Yang, X.; Zhou, R.; Pan, C.; Wang, Z. L. Enhanced Performances of Flexible ZnO/Perovskite Solar Cells by Piezo-Phototronic Effect. *Nano Energy* **2016**, *23*, 27−33.
(25) Pan, C.; Niu, S.; Ding, Y.; Dong, L.; Yu, R.; Liu, Y.; Zhu, G.; Wang, Z. L. Enhanced Cu_2S/CdS Coaxial Nanowire Solar Cells by Piezo-Phototronic Effect. *Nano Lett.* **2012**, *12*, 3302−3307.
(26) Yang, Y.; Guo, W.; Zhang, Y.; Ding, Y.; Wang, X.; Wang, Z. L. Piezotronic Effect on the Output Voltage of P3HT/ZnO Micro/Nanowire Heterojunction Solar Cells. *Nano Lett.* **2011**, *11*, 4812−4817.
(27) Zhu, L.; Wang, L.; Xue, F.; Chen, L.; Fu, J.; Feng, X.; Li, T.; Wang, Z. L. Piezo-Phototronic Effect Enhanced Flexible Solar Cells Based on n-ZnO/p-SnS Core−Shell Nanowire Array. *Adv. Sci.* **2016**, 1600185.
(28) Que, M.; Zhou, R.; Wang, X.; Yuan, Z.; Hu, G.; Pan, C. Progress in Piezo-Phototronic Effect Modulated Photovoltaics. *J. Phys.: Condens. Matter* **2016**, *28*, 433001.
(29) Zhang, Y.; Yang, Y.; Wang, Z. L. Piezo-Phototronics Effect on Nano/Microwire Solar Cells. *Energy Environ. Sci.* **2012**, *5*, 6850−6856.
(30) Wang, L.; Liu, S.; Wang, Z.; Zhou, Y.; Qin, Y.; Wang, Z. L. Piezotronic Effect Enhanced Photocatalysis in Strained Anisotropic ZnO/TiO_2 Nanoplatelets *via* Thermal Stress. *ACS Nano* **2016**, *10*, 2636−2643.
(31) Wu, W.; Wang, Z. L. Piezotronics and Piezo-Phototronics for Adaptive Electronics and Optoelectronics. *Nat. Rev. Mater.* **2016**, *1*, 16031.
(32) Zhang, Y.; Yan, X.; Yang, Y.; Huang, Y.; Liao, Q.; Qi, J. Scanning Probe Study on the Piezotronic Effect in ZnO Nanomaterials and Nanodevices. *Adv. Mater.* **2012**, *24*, 4647−4655.
(33) Zhang, X.-M.; Lu, M.-Y.; Zhang, Y.; Chen, L.-J.; Wang, Z. L. Fabrication of a High-Brightness Blue-Light-Emitting Diode Using a ZnO-Nanowire Array Grown on p-GaN Thin Film. *Adv. Mater.* **2009**, *21*, 2767−2770.
(34) Zhang, Z.; Liao, Q.; Yu, Y.; Wang, X.; Zhang, Y. Enhanced Photoresponse of ZnO Nanorods-Based Self-Powered Photodetector by Piezotronic Interface Engineering. *Nano Energy* **2014**, *9*, 237−244.
(35) Sze, S. M.; Ng, K. K. *Physics of Semiconductor Devices*. John Wiley & Sons: Hoboken, NJ, 2006.
(36) Gao, Y.; Wang, Z. L. Equilibrium Potential of Free Charge Carriers in a Bent Piezoelectric Semiconductive Nanowire. *Nano Lett.* **2009**, *9*, 1103−10.
(37) Shao, Z.; Wen, L.; Wu, D.; Zhang, X.; Chang, S.; Qin, S. Influence of Carrier Concentration on Piezoelectric Potential in a Bent ZnO Nanorod. *J. Appl. Phys.* **2010**, *108*, 124312.
(38) Wen, X.; Wu, W.; Wang, Z. L. Effective Piezo-Phototronic Enhancement of Solar Cell Performance by Tuning Material Properties. *Nano Energy* **2013**, *2*, 1093−1100.
(39) Wen, X.; Wu, W.; Ding, Y.; Wang, Z. L. Piezotronic Effect in Flexible Thin-Film Based Devices. *Adv. Mater.* **2013**, *25*, 3371−3379.

DOI: 10.1021/acsnano.6b07960
ACS Nano 2017, 11, 1894−1900